

# Sgr A\* near-infrared flares from reconnection events in a magnetically arrested accretion flow

J. Dexter,<sup>1,2\*</sup> A. Tchekhovskoy,<sup>3</sup> A. Jiménez-Rosales,<sup>2</sup> S. M. Ressler,<sup>4</sup> M. Bauböck,<sup>2</sup> Y. Dallilar,<sup>2</sup> P. T. de Zeeuw,<sup>2,5</sup> F. Eisenhauer,<sup>2</sup> S. von Fellenberg,<sup>2</sup> F. Gao,<sup>2</sup> R. Genzel,<sup>2,6</sup> S. Gillessen,<sup>2</sup> M. Habibi,<sup>2</sup> T. Ott,<sup>2</sup> J. Stadler,<sup>2</sup> O. Straub,<sup>2</sup> F. Widmann<sup>2</sup>

<sup>1</sup>JILA and Department of Astrophysical and Planetary Sciences, University of Colorado, Boulder, CO 80309, USA

<sup>2</sup>Max Planck Institute for Extraterrestrial Physics (MPE), Giessenbachstr. 1, 85748 Garching, Germany

<sup>3</sup>Center for Interdisciplinary Exploration & Research in Astrophysics (CIERA), Physics & Astronomy, Northwestern University, Evanston, IL 60202, USA

<sup>4</sup>Kavli Institute for Theoretical Physics, University of California Santa Barbara, Kohn Hall, Santa Barbara, CA 93107, USA

<sup>5</sup>Sterrewacht Leiden, Leiden University, Postbus 9513, 2300 RA Leiden, The Netherlands

<sup>6</sup>Departments of Physics and Astronomy, Le Conte Hall, University of California, Berkeley, CA 94720, USA

Accepted XXX. Received YYY; in original form ZZZ

## ABSTRACT

Large amplitude Sgr A\* near-infrared flares result from energy injection into electrons near the black hole event horizon. Dynamical signatures in astrometry show continuous rotation of the emission region during bright flares, and corresponding rotations of the linear polarization angle. One broad class of physical flare models invoke magnetic reconnection. Here we show that such a scenario can arise in a general relativistic MHD simulation of a magnetically arrested accretion flow. Saturation of flux on the black hole triggers magnetic “eruption” events. Dissipation via reconnection in such events is associated with increases in near-infrared emission in models of Sgr A\*. Such events occur at roughly the timescale to re-accumulate the flux from somewhat larger radius,  $\simeq 10h$  for Sgr A\*. We study NIR observables from one sample event to show that the emission morphology tracks the boundary of the magnetically dominated region. As the region rotates, the NIR centroid and polarization angle both undergo continuous rotation, similar to the behavior seen in Sgr A\* flares.

**Key words:** accretion, accretion discs — black hole physics — Galaxy: centre — MHD — polarization — radiative transfer

## 1 INTRODUCTION

The Galactic center massive black hole Sgr A\* shows variable near-infrared (NIR) emission with factor  $\sim 10$  increases (Genzel et al. 2003; Ghez et al. 2004) over its median value (Schödel et al. 2011; Dodds-Eden et al. 2011; Witzel et al. 2018). The so-called “flares” are often accompanied by simultaneous events in the X-ray (Baganoff et al. 2001; Eckart et al. 2008b; Marrone et al. 2008). The lack of a clear submillimeter counterpart implies that flares are due to particle heating rather than an increase of the mass accretion rate (Markoff et al. 2001). The  $\simeq 10 - 40\%$  linear polarization seen in NIR flares is a signature of synchrotron radiation (Eckart et al. 2006; Trippe et al. 2007; Eckart et al. 2008a). Despite nearly 2 decades of study, their physical origin remains uncertain.

Recently, NIR long baseline interferometry with the VLT Interferometer instrument GRAVITY (Gravity Collaboration et al. 2017) showed a continuous rotation of the NIR centroid during 3 bright

flares with apparent periods of  $\simeq 30 - 60$  minutes (Gravity Collaboration et al. 2018). The observed motion is consistent with models of a compact orbiting emission region (Broderick & Loeb 2005, 2006) at a radius of  $r \simeq 6 - 10r_g$  (Gravity Collaboration et al. 2020, but see Matsumoto et al. 2020). Simultaneous rotation of the linear polarization angle with a comparable period are consistent with the same scenario, as long as there is a significant poloidal magnetic field component in the emission region (Gravity Collaboration et al. 2018, Gravity Collaboration et al., 2020, in prep).

Radiative models based on general relativistic MHD (GRMHD) simulations of Sgr A\* accretion are consistent with the source spectrum, image sizes, and image-integrated polarization properties (Mościbrodzka et al. 2009, 2014; Dexter et al. 2009, 2010; Shcherbakov et al. 2012; Chan et al. 2015a; Ressler et al. 2017; Chael et al. 2018; Anantua et al. 2020). In some cases, the models produce sufficiently hot electrons to match the observed NIR luminosity (e.g., Dexter & Fragile 2013; Chan et al. 2015b; Ressler et al. 2017). The NIR emission region is usually found to

\* jason.dexter@colorado.edu

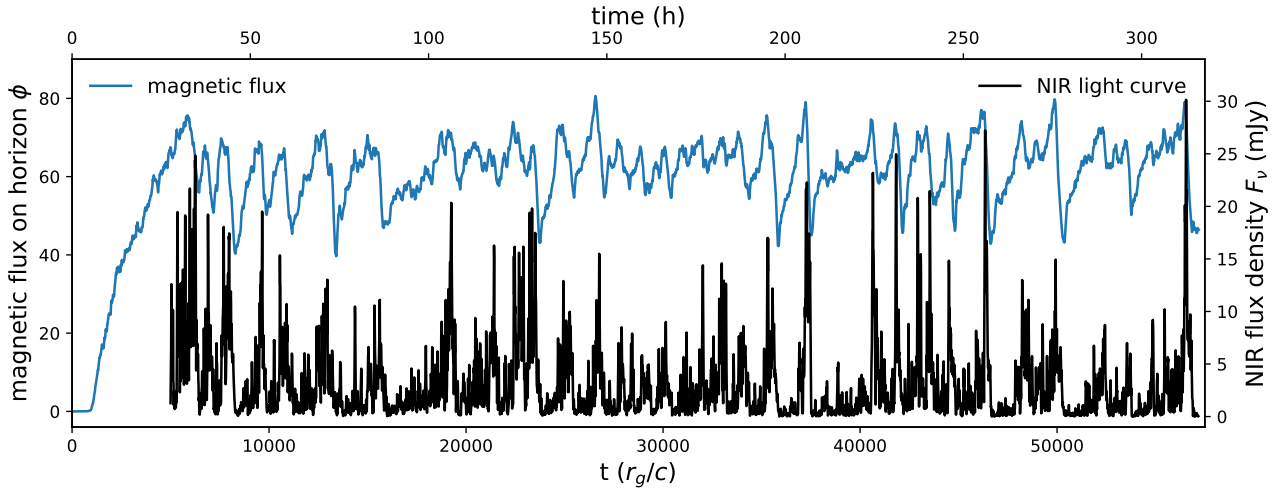


**Figure 1.** Magnetic flux accumulated on the event horizon as a function of time (blue) and the corresponding near-infrared light curve (black) for the long duration MAD simulation studied here. The magnetic flux shows cycles of gradual ramp up and rapid dissipation. The dissipation events are due to magnetic flux eruptions from near the black hole, and are associated with large-amplitude near-infrared variability. Such “flares” occur every  $\approx 10$  h for Sgr A\*. We have re-scaled the NIR light curve such that  $F_\nu \propto \dot{M}^2$  with  $\dot{M}$  being the temporally smoothed accretion rate through the horizon. This keeps the median flux density roughly constant as the mass reservoir drains.

be concentrated close to the black hole event horizon (e.g., Dolence et al. 2009; Ressler et al. 2017; Petersen & Gammie 2020).

Here we consider a scenario for Sgr A\* flares as the result of stochastic, repeating, large-scale magnetic reconnection occurring in GRMHD models of magnetically arrested disks (MADs, Igumenshchev et al. 2003; Narayan et al. 2003; Tchekhovskoy et al. 2011; McKinney et al. 2012). We study one GRMHD model which we found to be broadly consistent with observations of Sgr A\* (Dexter et al. 2020). We show that NIR flares occur every  $\approx 10$  h in the same models as the result of magnetic eruptions originating close to the black hole (section 2). The flares show continuous rotation of the astrometric centroid as a result of rotating spiral structure in the emission region (section 3). We find a corresponding rotation of the polarization angle due to the strong poloidal fields near the black holes. We discuss limitations of the current model and implications for our understanding of accretion onto Sgr A\* (section 4).

## 2 FLUX ERUPTIONS IN NUMERICAL MODELS OF MADS

Here we study one long duration, MAD GRMHD simulation described in Dexter et al. (2020) and run with the `harmpli`<sup>1</sup> code (Tchekhovskoy 2019). The  $320 \times 256 \times 160$  simulation was run for a time of  $6 \times 10^4 r_g/c$  after being initialized from a Fishbone-Moncrief torus with inner radius  $r_{\text{in}} = 12r_g$ , pressure maximum radius  $r_{\text{max}} = 25r_g$ , and black hole spin parameter of  $a = 0.9375$ . A single poloidal loop of magnetic field particularly designed to supply a large amount of magnetic flux was added such that  $\max(p_g)/\max(p_B) = 100$ , where  $p_g$  and  $p_B$  are the gas and magnetic pressures (see, e.g., Tchekhovskoy et al. 2011). By the end of the run, inflow equilibrium was established out to  $r \approx 90r_g$ . The simulation included a scheme for self-consistently evolving four separate electron internal energy densities along with that of the single MHD fluid (Ressler et al. 2015). Each electron energy used

a different, sub-grid heating prescription based on kinetics calculations. Here we focus on the magnetic reconnection model of Werner et al. (2018), which can produce both the median NIR flux density and large-amplitude flaring behavior. The results presented here for electron heating during magnetic flux disruptions are consistent across all electron models.

Figure 1 shows the dimensionless magnetic flux accumulated on the horizon as a function of time,  $\phi = \sqrt{4\pi}\Phi_{\text{BH}}/\sqrt{\dot{M}}$ , where  $\Phi_{\text{BH}}$  is the magnetic flux and  $\dot{M} > 0$  is the accretion rate which we smooth over timescales of  $1000 r_g/c$ . Magnetic flux is advected inwards with the flow and rapidly builds up on the event horizon, saturating in a MAD state where  $\phi \approx 50 - 60$  (e.g., Tchekhovskoy et al. 2011; McKinney et al. 2012). The normalized magnetic flux undergoes cycles of gradual build up and rapid dissipation. The dissipation events are due to stochastic magnetic flux “eruption” events from near the black hole (Igumenshchev 2008). They recur after the time required to reach the saturated state following a dissipation event.

These magnetic flux eruptions launch low-density tubes of magnetic flux which form a rotating spiral pattern (Igumenshchev 2008; Tchekhovskoy et al. 2011). Figure 2 shows vertically averaged maps of particle density, electron temperature, and plasma  $\beta$  at four snapshots near the  $7 - 8 \times 10^3 r_g/c$  event. Hot, strongly magnetized, low density plasma forms a spiral structure which rotates continuously around the black hole at small radii of  $r \lesssim 10r_g$ . Similar non-axisymmetric spirals are seen in all eruption events.

## 3 NEAR-INFRARED OBSERVABLES

We calculate NIR observables from the time period corresponding to this magnetic flux eruption event. The second to last row of Figure 2 shows vertically-averaged maps of the NIR emissivity, using the simulation data scaled to cgs units and the angle-dependent synchrotron emissivity fitting function from Mahadevan et al. (1996). The coordinate frame emissivity tracks the morphology of the eruption event, with emission coming particularly from the boundary between the strongly magnetized, low density and more weakly magnetized, higher density regions.

<sup>1</sup> <https://github.com/atcekho/harmpli>

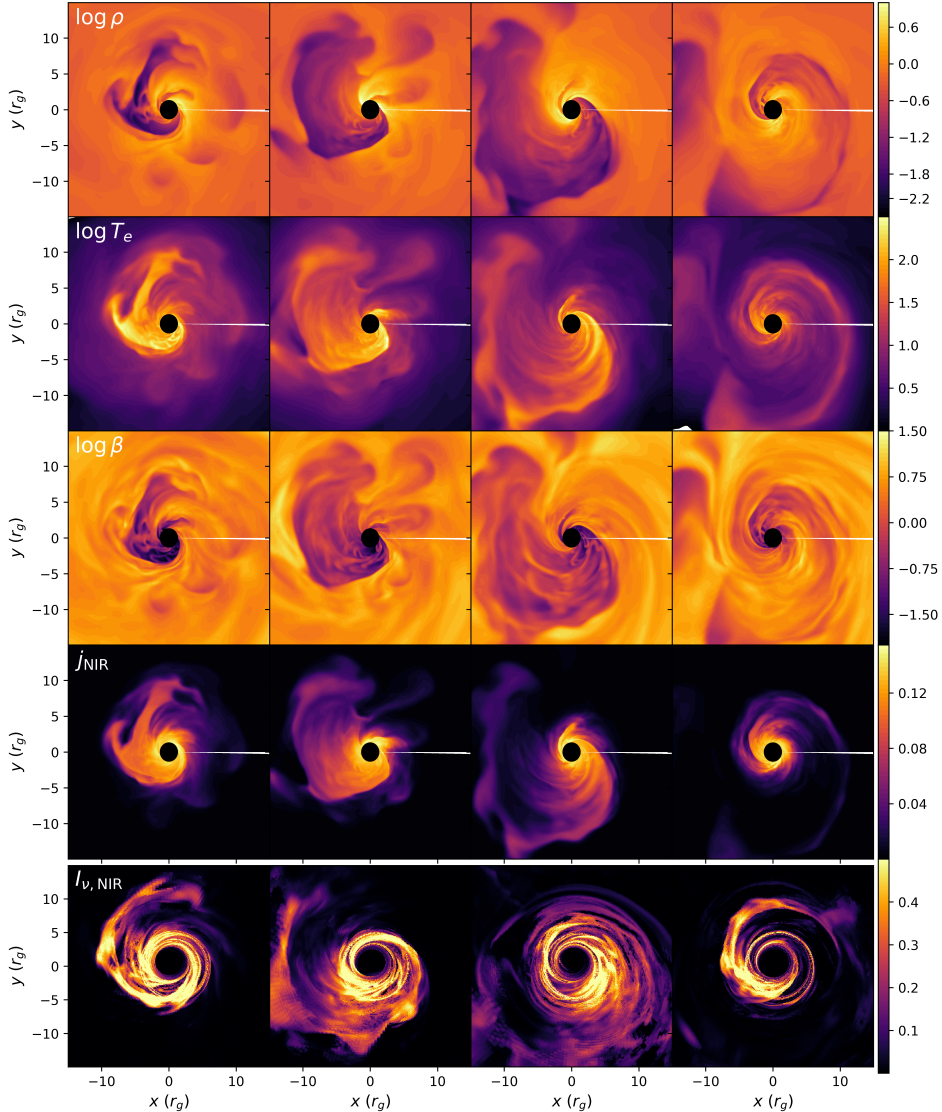


**Figure 2.** Vertically averaged maps of simulation variables of density, electron temperature, plasma  $\beta$ , and their coordinate frame NIR emissivity at four snapshots spanning the flare period of 320 – 400 minutes. Ray traced NIR images are shown in the bottom row. The rotating, spiral morphology of the flaring region matches that of the low  $\beta$ , high  $T_e$  regions corresponding to the MAD magnetic flux eruptions. [JD: add unit description here or as labels.](#)

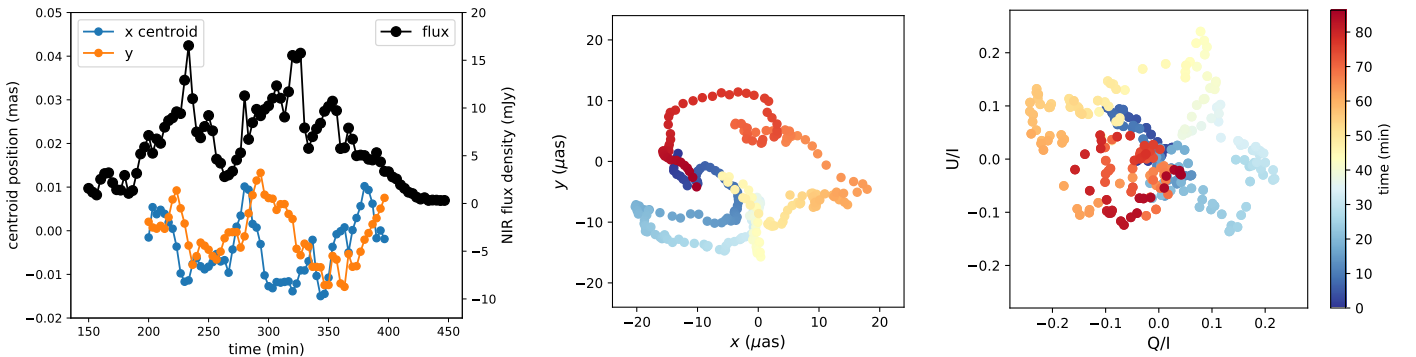


**Figure 3.** Left: Total NIR flux density (black) and x and y image centroid positions (blue and orange) as a function of time during one MAD reconnection event. The rapid, large amplitude variability is accompanied by rotation in the centroid, particularly during the end of the flare from  $\approx 320$  – 400 minutes. The NIR x and y total intensity centroid positions (middle) and  $Q/I$ ,  $U/I$  polarization fractions (right) are shown color-coded in time from blue to yellow to red over the period of 320 – 400 minutes of the flare from the left panel. The NIR centroid rotates continuously with an astrometric period of  $\approx 80$  minutes. At the same time, the polarization angle rotates with a comparable period.

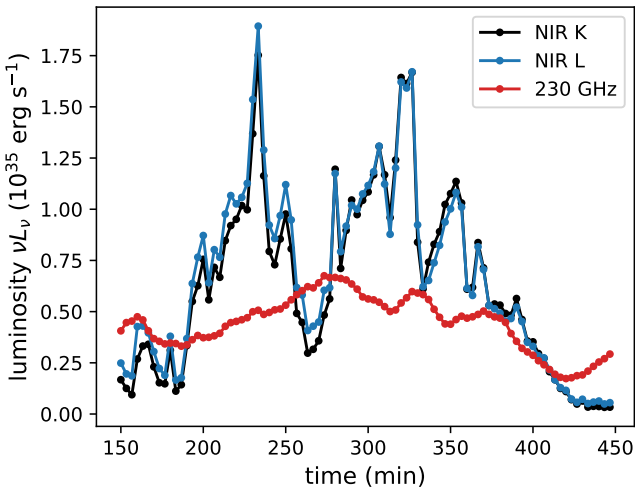


**Figure 4.** K ( $2.2 \mu\text{m}$ ) and L ( $3.8 \mu\text{m}$ ) NIR and 1.3mm light curves during the flare studied here. The NIR spectral index in  $\nu L_\nu$  varies between  $\approx -1$ – $-0.2$ . The submm light curve shows its typical factor  $\approx 50\%$  variability, without any clear simultaneous changes corresponding to the NIR flares.

We then calculate polarized movies using the `grtrans`<sup>2</sup> code (Dexter et al. 2009; Dexter 2016) including all relativistic effects. We fix the observer inclination angle at  $i = 25^\circ$ , consistent with GRAVITY results (Gravity Collaboration et al. 2018, Gravity Collaboration et al., 2020, in prep.). Images are calculated with a field of view of  $130 \mu\text{as}$  with  $300 \times 300$  pixels. As in Dexter et al. (2020), we remove emission from the most highly magnetized regions with  $b^2/\rho > 1$ . We fix the mass of Sgr A\* at  $M = 4 \times 10^6 M_\odot$  with a distance to the Galactic center of 8 kpc (e.g., Ghez et al. 2008; Gillessen et al. 2009; Gravity Collaboration et al. 2019; Do et al. 2019; Gravity Collaboration et al. 2020).

The last row of Figure 1 shows the NIR model light curve over a continuous  $\approx 300$ h time interval for Sgr A\*. Strong peaks in near-infrared flux density are apparent, each corresponding to a decrease in magnetic flux on the event horizon. Sample snapshot images are shown in the last row of Figure 2. The spiral morphology matches that in the coordinate frame simulation data of the same flare, and the emission region rotates continuously completing one full period over this time span. The left panel of Figure 3 shows one double-peaked K band ( $2.2 \mu\text{m}$ ) NIR flare corresponding to the time period of the eruption event studied above. The  $x$  and  $y$  centroids also show motion suggestive of rotation, with an on sky diameter of  $\lesssim 25 \mu\text{as}$ . We show the astrometric motion on sky and the polarized properties in the middle and right panels. Here we use simulation data spaced by  $\Delta t = 20$ s and account for light travel time delays through the emission region. The NIR centroid rotates continuously over the 80 minutes, accompanied by a single rotation of the polarization angle showing up as a “loop” in the Stokes parameters  $Q$  and  $U$ .

Finally, Figure 4 compares NIR K and L band light curves with that at 1.3mm (230 GHz). The spectral index is variable during the flare but fairly flat, ranging from values of  $\beta \approx -1$ – $-0.2$  for  $\nu L_\nu \sim \nu^\beta$ . There is no simultaneous, sharp rise in submm flux during the NIR flaring event. However, the flux eruption disrupts the entire inner accretion flow. In future work we will explore structural variability associated with these events.

Where does the emission originate? The flux eruptions are associated with magnetically dominated, low density material. Synchrotron radiation scales with density, and we explicitly exclude emission from highly magnetized regions where  $b^2/\rho > 1$ . The observed emission morphology tracks that of the magnetized material, but originates from its interface with the rest of the fluid. Typical fluid properties calculated as intensity-weighted averages are  $n \approx 10^6 \text{ cm}^{-3}$ ,  $B \approx 100 \text{ G}$ ,  $T_e \approx 10^{12} \text{ K}$ ,  $\beta \approx 5$ . While low density, strongly magnetized, and hot compared to submm emitting electrons in the same models, the bulk of the radiation does not originate from magnetically dominated plasma. If we instead apply a cut where  $b^2/\rho > 25$ , the flux density increases by a factor  $\approx 2$ . The average properties of radiating electrons all change by a similar amount, e.g. the new emission comes from more highly magnetized material. The emission region morphology, centroid motion, and polarization behavior remain the same.

## 4 DISCUSSION

We have shown that flux eruption events associated with magnetically arrested accretion flows result in highly non-axisymmetric, magnetically dominated regions which travel outwards, disrupt the accretion flow, and cause plasma heating via magnetic reconnection. By calculating NIR observables of Sgr A\* from one example simulation, we have shown that such events trigger large-amplitude near-infrared variability that resemble many observed properties of the NIR/X-ray “flares”:

- a factor of  $\approx 10$ – $20$  increases in flux density compared to the median with durations of  $\approx 30$ – $60$  minutes;
- a recurrence timescale of several hours;
- a flat spectral index in the NIR, without a simultaneous submillimeter counterpart;
- linear polarization fractions of  $\approx 10$ – $20\%$ ;
- continuous rotation of the emission region accompanied by a rotation of the linear polarization angle.

These flaring events occur in a model which satisfies many other Sgr A\* submm to NIR observational constraints (Dexter et al. 2020). The flare recurrence time is the timescale for magnetic flux to accumulate on the black hole and saturate following a dissipation event. The flares are driven primarily by increases in electron temperature due to particle heating from magnetic reconnection. The polarization oscillation is due to the stable, strong poloidal magnetic field in the inner MAD accretion flow (Gravity Collaboration et al. 2018).

Compared to the observed Sgr A\* NIR flares, i) the flux distribution shows too many moderate and not enough very bright flares (The GRAVITY Collaboration et al. 2020), ii) the flare spectra might be too steep (too “red”), iii) the astrometric and polarization periods are at the long end of the observed range, and iv) the size of the astrometric pattern on sky is a factor of  $\approx 2$  too small.

The physical model is also overly simplistic. We assume a purely thermal distribution of electrons, while relativistic magnetic reconnection can produce significant non-thermal particle acceleration (e.g., Sironi & Spitkovsky 2014; Guo et al. 2015; Werner et al. 2016). The cooling time given the typical parameters of our radiating electrons is  $\sim 10$  min, similar to the dynamical time close to the black hole and shorter than the flare duration. Radiative cooling may be important, particularly if higher energy non-thermal electrons contribute significantly to the observed flux. Due to our inclusion of only thermal electrons and our neglect of Compton

<sup>2</sup> <https://github.com/jadexter/grtrans>

scattering, we are at present unable to make predictions for the X-ray luminosity or spectra of the flaring events studied here.

MAD models generically produce strongly magnetized regions which are difficult to evolve accurately in ideal GRMHD simulations such as those used here. Flux eruptions are particularly difficult in this regard, since they produce steep gradients in magnetization over a large part of the inner accretion flow. Our results qualitatively match those in previous MAD simulations (e.g., Tchekhovskoy et al. 2011; White et al. 2019). We have also carried out otherwise identical simulations at lower resolutions of 3/4 and 1/2 the number of cells in each dimension. The flow structure and the time evolution of ramp up and dissipation cycles in magnetic flux are consistent in all cases. Many individual disruptions also look very similar between the full and 3/4 resolution cases in terms of vertically integrated maps (Figure 2). Still, the robustness of the (thermo)dynamics of such events to changes in resolution, code floors, or the grid scale dissipation in ideal MHD remains uncertain.

We find that NIR centroid motions are larger during flares than otherwise. All flares in the long duration simulation are associated with some degree of continuous rotation, showing apparent periods of 40 – 100 min and completing 1/2 – 2 rotations. The observed rotation speed is consistent with the (sub-Keplerian) orbital speed at  $r \approx 4 - 8 r_g$ , comparable to the outer radius of the magnetically dominated structure during flares. We do not find correlations between centroid size or astrometric period and the total radiated energy or peak flux during a flare. We also see similar periods and centroid excursions in a small number of flux eruption events in shorter duration  $a = 0$  and  $a = 0.5$  simulations. According to our model, future flares should show a range of periods and astrometric sizes. In higher precision data, the centroid track would appear more complex than that of a compact region undergoing orbital motion.

In our models, there is an average  $\lesssim 10 \mu\text{as}$  offset between the NIR emission region centroid and the position of the black hole. The offset is in the direction of approaching material, and results from Doppler beaming due to relativistic motion. Since our models underproduce the observed amplitude of centroid motion seen in NIR flares, we consider this a lower limit to the bias that would be induced in GRAVITY astrometric measurements in the S2 orbit in 2017 and 2018. This level of bias currently leads to a negligible error in parameters inferred from the orbit of S2 (GRAVITY Collaboration et al. 2020).

The flares seen here are a direct consequence of strong magnetic fields near the black hole event horizon, which becomes dynamically important and repels accreting gas. The existence of such a flow structure near Sgr A\* may be a natural consequence of the accretion of weakly magnetized stellar winds in the central parsec (Ressler et al. 2019, Ressler et al. 2020, submitted).

Although the total submm intensity does not vary simultaneously with that of the NIR, our models do show rotations of the submm polarization angle during the flares. Similar features have been seen in submm polarimetry data (e.g., Moran et al. 2007). Since the flux eruption events disrupt the inner accretion flow, we generically expect that NIR flares should be accompanied by observable signatures in resolved submm images with the Event Horizon Telescope (Event Horizon Telescope Collaboration et al. 2019).

## ACKNOWLEDGEMENTS

J.D. and A.J.-R. were supported in part by a Sofja Kovalevskaja award from the Alexander von Humboldt foundation, by a CONACYT/DAAD grant (57265507), and by NASA Astrophysics Theory

Program Grant 80NSSC20K0527. S.M.R. is supported by the Gordon and Betty Moore Foundation through Grant GBMF7392. The calculations presented here were carried out on the MPG supercomputers Hydra and Cobra hosted at MPCDF, and using resources supported by the NASA High-End Computing (HEC) Program through the NASA Advanced Supercomputing (NAS) Division at Ames Research Center.

## REFERENCES

- Anantua R., Ressler S., Quataert E., 2020, *MNRAS*,
- Baganoff F. K., et al., 2001, *Nature*, **413**, 45
- Broderick A. E., Loeb A., 2005, *MNRAS*, **363**, 353
- Broderick A. E., Loeb A., 2006, *ApJ*, **636**, L109
- Chael A., Rowan M., Narayan R., Johnson M., Sironi L., 2018, *MNRAS*, **478**, 5209
- Chan C.-K., Psaltis D., Özel F., Narayan R., Sadowski A., 2015a, *ApJ*, **799**, 1
- Chan C.-k., Psaltis D., Özel F., Medeiros L., Marrone D., Sadowski A., Narayan R., 2015b, *ApJ*, **812**, 103
- Dexter J., 2016, *MNRAS*, **462**, 115
- Dexter J., Fragile P. C., 2013, *MNRAS*, **432**, 2252
- Dexter J., Agol E., Fragile P. C., 2009, *ApJ*, **703**, L142
- Dexter J., Agol E., Fragile P. C., McKinney J. C., 2010, *ApJ*, **717**, 1092
- Dexter J., et al., 2020, arXiv e-prints, p. [arXiv:2004.00019](https://arxiv.org/abs/2004.00019)
- Do T., et al., 2019, *Science*, **365**, 664
- Dodds-Eden K., et al., 2011, *ApJ*, **728**, 37
- Dolence J. C., Gammie C. F., Mościbrodzka M., Leung P. K., 2009, *ApJS*, **184**, 387
- Eckart A., Schödel R., Meyer L., Trippe S., Ott T., Genzel R., 2006, *A&A*, **455**, 1
- Eckart A., et al., 2008a, *A&A*, **479**, 625
- Eckart A., et al., 2008b, *A&A*, **492**, 337
- Event Horizon Telescope Collaboration et al., 2019, *ApJ*, **875**, L2
- GRAVITY Collaboration et al., 2020, arXiv e-prints, p. [arXiv:2004.07187](https://arxiv.org/abs/2004.07187)
- Genzel R., Schödel R., Ott T., Eckart A., Alexander T., Lacombe F., Rouan D., Aschenbach B., 2003, *Nature*, **425**, 934
- Ghez A. M., et al., 2004, *ApJ*, **601**, L159
- Ghez A. M., et al., 2008, *ApJ*, **689**, 1044
- Gillessen S., Eisenhauer F., Trippe S., Alexander T., Genzel R., Martins F., Ott T., 2009, *ApJ*, **692**, 1075
- Gravity Collaboration et al., 2017, *A&A*, **602**, A94
- Gravity Collaboration et al., 2018, *A&A*, **618**, L10
- Gravity Collaboration et al., 2019, *A&A*, **625**, L10
- Gravity Collaboration et al., 2020, *A&A*, **635**, A143
- Guo F., Liu Y.-H., Daughton W., Li H., 2015, *ApJ*, **806**, 167
- Igumenshchev I. V., 2008, *ApJ*, **677**, 317
- Igumenshchev I. V., Narayan R., Abramowicz M. A., 2003, *ApJ*, **592**, 1042
- Mahadevan R., Narayan R., Yi I., 1996, *ApJ*, **465**, 327
- Markoff S., Falcke H., Yuan F., Biermann P. L., 2001, *A&A*, **379**, L13
- Marrone D. P., et al., 2008, *ApJ*, **682**, 373
- Matsumoto T., Chan C.-H., Piran T., 2020, arXiv e-prints, p. [arXiv:2004.13029](https://arxiv.org/abs/2004.13029)
- McKinney J. C., Tchekhovskoy A., Blandford R. D., 2012, *MNRAS*, **423**, 3083
- Moran J. M., Marrone D. P., Zhao J. H., Rao R., 2007, in Aschenbach B., Burwitz V., Hasinger G., Leibundgut B., eds, Relativistic Astrophysics Legacy and Cosmology - Einstein's Legacy. p. 163, doi:[10.1007/978-3-540-74713-0\\_37](https://doi.org/10.1007/978-3-540-74713-0_37)
- Mościbrodzka M., Gammie C. F., Dolence J. C., Shiokawa H., Leung P. K., 2009, *ApJ*, **706**, 497
- Mościbrodzka M., Falcke H., Shiokawa H., Gammie C. F., 2014, *A&A*, **570**, A7
- Narayan R., Igumenshchev I. V., Abramowicz M. A., 2003, *PASJ*, **55**, L69
- Petersen E., Gammie C., 2020, *MNRAS*,

## 6 *Dexter, Tchekhovskoy, Jiménez-Rosales, Ressler, et al.*

Ressler S. M., Tchekhovskoy A., Quataert E., Chand ra M., Gammie C. F., 2015, [MNRAS](#), **454**, 1848

Ressler S. M., Tchekhovskoy A., Quataert E., Gammie C. F., 2017, [MNRAS](#), **467**, 3604

Ressler S. M., Quataert E., Stone J. M., 2019, [MNRAS](#), **482**, L123

Schödel R., Morris M. R., Muzic K., Alberdi A., Meyer L., Eckart A., Gezari D. Y., 2011, [A&A](#), **532**, A83

Shcherbakov R. V., Penna R. F., McKinney J. C., 2012, [ApJ](#), **755**, 133

Sironi L., Spitkovsky A., 2014, [ApJ](#), **783**, L21

Tchekhovskoy A., 2019, HARMPI: 3D massively parallel general relativistic MHD code (ascl:1912.014)

Tchekhovskoy A., Narayan R., McKinney J. C., 2011, [MNRAS](#), **418**, L79

The GRAVITY Collaboration et al., 2020, arXiv e-prints, p. [arXiv:2004.07185](#)

Trippe S., Paumard T., Ott T., Gillessen S., Eisenhauer F., Martins F., Genzel R., 2007, [MNRAS](#), **375**, 764

Werner G. R., Uzdensky D. A., Cerutti B., Nalewajko K., Begelman M. C., 2016, [ApJ](#), **816**, L8

Werner G. R., Uzdensky D. A., Begelman M. C., Cerutti B., Nalewajko K., 2018, [MNRAS](#), **473**, 4840

White C. J., Stone J. M., Quataert E., 2019, [ApJ](#), **874**, 168

Witzel G., et al., 2018, [ApJ](#), **863**, 15

This paper has been typeset from a  $\text{\TeX}/\text{\LaTeX}$  file prepared by the author.